ORIGINAL PAPER

The intrinsic origin of the grain-boundary resistance in Sr-doped LaGaO$_3$

Sangtae Kim

Abstract In this paper I summarize our recent investigations (Park and Kim, Phys Chem C 111:14903, 2007; Solid State Ionics 179:1329, 2008) on the origin of the grain-boundary resistance in a doped LaGaO$_3$, a perovskite-structured solid electrolyte. The partial electronic and ionic resistances of the bulk and the grain boundaries, as well as the total resistance, in 1 mol% Sr-doped LaGaO$_3$ were measured separately by means of a dc-polarization method and ac-impedance spectroscopy. Both of the partial resistances at the grain boundaries were greater than the bulk counterparts, indicating that the grain boundaries impede the ionic as well as the electronic transport in this material. The transference number of the partial electronic conductivity at the grain boundary was however greater than that in the bulk. This fact strongly suggests that both electronic and ionic charge carriers deplete at the grain boundaries to form the space-charge zones and that the grain-boundary cores in this material are positively charged. In light of the fact that the effective charge of the oxygen vacancy ($+2$) is greater than that of the electron hole ($+1$), the oxygen vacancies deplete more sharply in the space-charge zones compared to the electron holes such that the grain boundaries become more mixed conducting relative to the bulk. These observations verify that the electrical conduction across the grain-boundaries in 1 mol% Sr-doped LaGaO$_3$ is governed by the space charge.

S. Kim (✉)
Department of Chemical Engineering and Materials Science,
University of California, Davis, CA 95616, USA
e-mail: chmkim@ucdavis.edu

Introduction

The physical behavior of grain boundaries (i.e., interfaces between crystallites, namely grains, in polycrystalline ceramics) differs from that of the bulk due to their structural deviation from the crystal interior. In the past decade, the electrical nature of grain boundaries relative to the bulk has attracted considerable attention as "size effects" [1] on the conductivity have become one of the main foci of research interest, particularly in the field of solid state ionics. Reducing the size of the grains enhances the geometric contribution of the grain boundaries to the total volume of the polycrystalline ceramic such that the overall electrical properties may be governed by the property associated with the grain boundaries when the grain size is sufficiently small (typically less than few tens of nanometers). The overall conductivity of a material with a higher density of grain boundaries can then be enhanced if the grain boundaries serve as highly conducting paths.

Solid electrolytes (SEs) [2] are virtually pure ionic conductors that serve as a key component in electrochemical devices such as solid oxide fuel cells (SOFCs) [3, 4]. Among them, doped zirconia and ceria, fast oxygen-ionic conductors with a fluorite structure, have almost exclusively been employed as SEs for SOFC applications owing to their relatively high ionic conductivity at elevated temperatures [2–4]. However, these SEs present sufficiently high ionic conductivity only at very high temperatures, leading to the high operating temperature (>800 °C) of the SOFCs. It is desirable to lower the

operating temperature down to the intermediate temperature (IT) range (500–700 °C or even less) to ameliorate the problems associated with high-temperature operation, such as long-term durability of the cells and cost [4]. Lower-temperature operation, on the other hand, requires enhanced conductance in the SEs.

Nanocrystalline SEs have been the center of attention for over a decade owing to their potential for use in the IT-SOFCs. However, it was found that the grain boundaries in fluorite-structured SEs inherently rather impede oxygen-ionic transport in the materials, and this issue worsens at lower temperatures. Hence, the electrical nature of the grain boundaries in those SEs has been intensively explored during the past decade and the intrinsic origins of the grain boundary resistance are now relatively well understood [5–9]: at the grain boundaries, the oxygen vacancies ($V_O^{\bullet\bullet}$) deplete to form space-charge zones [10, 11] in the vicinity of the grain-boundary core, leading to high resistance to oxygen-ionic transport across them. The excess positive charge formed in the grain-boundary core is responsible for the depletion of $V_O^{\bullet\bullet}$ in the space-charge zones.

Doped LaGaO$_3$ is a perovskite-structured oxygen-ionic conductor that presents a conductivity higher than the conductivities of the fluorite-structured SEs at lower temperatures [12], and is thus considered a SE for IT-SOFC applications. However, the electrical nature of the grain boundaries in this SE resembles that in fluorite-structured SEs in that the grain boundaries block the oxygen-ionic transport. In view of the relatively recent discovery of this SE, research on it has focused almost exclusively on its bulk properties, while little attention has been paid to the grain boundaries to date. The chief question about the blocking nature of the grain boundaries in this perovskite-structured SE is whether the intrinsic cause of the grain-boundary resistance is the space charge, as seen in the fluorite-structured SEs.

In this contribution I summarize our recent investigations [13, 14] on the influence of the space-charge effects on the grain-boundary conduction in 1 mol% Sr-doped LaGaO$_3$ (LSGO), which we selected as a model system. As will be presented below, the results obtained from dc-polarization and ac-impedance measurements clearly demonstrate that both $V_O^{\bullet\bullet}$ and the electron holes (h$^{\cdot}$) (i.e., the majority charge carriers in LSGO at the oxygen partial pressure, P_{O_2}, of concern) deplete at the grain boundaries to form space-charge zones, leading to grain boundaries with high resistance to both ionic and the electronic transport across them.

Results and discussion

Figure 1 shows a high-resolution transmission electron microscope (HR-TEM) image of dense (>95%) LSGO
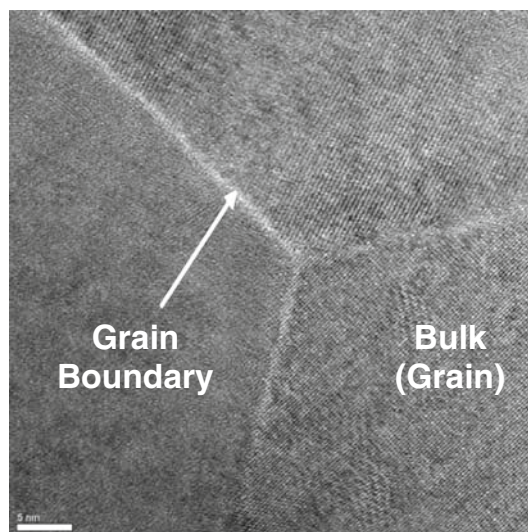

Fig. 1 A representative HR-TEM image of a dense (>95%) LSGO ceramic prepared for electrical measurements. The grain size is ~5 μm. The scale bar indicates 5 nm

used for electrical measurements. The grain boundaries appear to be free of pores as well as insulating amorphous phases which are often responsible for the high resistance to the ionic current at the grain boundaries observed in impure SEs. The Ca and Si contents (typical sources of the amorphous phases) in the sample, measured using an inductively coupled plasma (ICP) technique, were below the detection limit (≪100 ppm), consistent with the TEM results.

The resistances under different P_{O_2} in LSGO were measured using both ac-impedance spectroscopy and a dc-measurement technique. The advantage of the ac over the dc measurements is that the ac technique allows one to measure the local resistance (e.g., in the bulk and the grain boundary) separately. Figure 2 shows an ac-impedance spectrum (i.e., a Nyquist plot) measured from LSGO in O$_2$ at 400 °C (see red symbols), which consists of a relatively tiny (see also the inset in Fig. 2) arc that appears at higher frequencies and a large semicircular arc that subsequently appears at lower frequencies of concern (namely arc 1 and arc 2, respectively). Arc 1 appears to be incomplete. The best fits for arcs 1 and 2 using an equivalent circuit consisting of two parallel RQ elements in series [i.e., $(R_1Q_1)(R_2Q_2)$ where R and Q denote resistance and a constant-phase element, respectively] are indicated as solid lines in Fig. 2. The dielectric constant of ~30 at 400 °C estimated from C_1 ($=(R_1^{1-n}Q_1)^{1/n}$) agrees well with that of pure LaGaO$_3$ (~25) [15], suggesting that arcs 1 and 2 represent the bulk and the grain boundaries, respectively, as usual. (Figure 2 also shows an indication of a third arc, corresponding to the electrode resistance, which appears at at even lower frequency range than the frequency range of
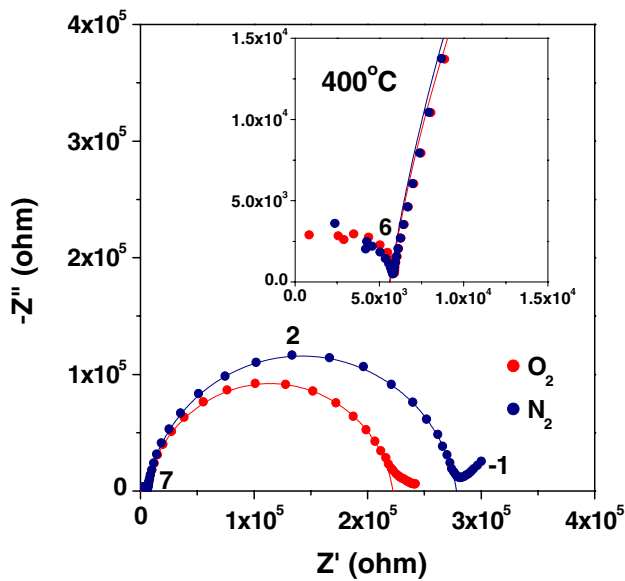
Fig. 2 Nyquist plots measured from LSCO under O_2 (*red symbols*) and N_2 (*blue symbols*) at 400 °C. The *inset* presents the plot at high frequencies. The *solid lines* indicate the best fits obtained using an equivalent circuit consisting of two parallel RQ elements

concern in this study; however, a discussion of the electrode resistance is beyond the scope of this paper.) Note that the grain boundaries are almost exclusively responsible for the overall resistance in LSGO at 400 °C. Figure 2 also shows a spectrum measured under N_2.

It is interesting to note that arc 2 varies with varying ambient P_{O_2}, while arc 1 remains unchanged. As mentioned above, the majority ionic and electronic charge carriers in LSGO under oxidizing conditions (e.g., under O_2) are $V_O^{\bullet\bullet}$ and $h^{\bullet}$, respectively. If electric conduction in LSGO is predominantly controlled by $V_O^{\bullet\bullet}$, the resistance should be independent of P_{O_2} since the number of $V_O^{\bullet\bullet}$ in the material is determined by the amont of dopant. Hence, the fact that only the grain-boundary resistance depends on the ambient P_{O_2} implies that the electronic contribution to grain-boundary conduction is greater than that the electronic contribution to the bulk conduction. In other words, the electronic transference number ($t_j = \sigma_j / \sum_k \sigma_k$) at the grain boundaries ($t_{el,gb}$) is greater than that in the bulk ($t_{el,\infty}$).

According to Eq. 1, at equilibrium, the local concentration of defect j in the vicinity of the grain-boundary core is determined by the electrical potential of the grain-boundary core:

$$\left(\frac{c_j(x)}{c_{j\infty}}\right)^{1/z_j} = \exp\left(-\frac{e}{k_B T}\Delta\phi(x)\right) \quad (1)$$

where $\Delta\phi(x)$ is the electrical potential relative to the bulk (subscript ∞; i.e., $\Delta\phi(x) = \phi(x) - \phi(\infty)$). The symbols z, e, k_B and T denote the charge number, elementary charge,

Boltzmann's constant and temperature, respectively. Both $V_O^{\bullet\bullet}$ and $h^{\bullet}$ thus deplete in the vicinity of the grain-boundary core to form space-charge zones if $\phi(0) > 0$. Furthermore, $V_O^{\bullet\bullet}$ should deplete more sharply than $h^{\bullet}$ (see Eq. 1), as illustrated qualitatively in Fig. 3, since the effective charge of $V_O^{\bullet\bullet}$ (+2) is greater than that of $h^{\bullet}$ (+1), leading to a greater $t_{el,gb}$ than $t_{el,\infty}$. Therefore, Fig. 2 strongly suggests that the grain-boundary conduction in LSGO is controlled by the space charge. In order to verify this speculation, one should measure the partial ionic and electronic conductivities at the grain boundaries and in the bulk separately to check whether $t_{el,gb}$ is in fact greater than $t_{el,\infty}$.

Figure 4 presents the current (I)–voltage (U) characteristics measured from an ion-blocking dc-polarization cell (see the inset in Fig. 4) at 475 °C in air. Dc-polarization methods [16, 17] are considered to be one of the most effective means to measure the partial conductivities
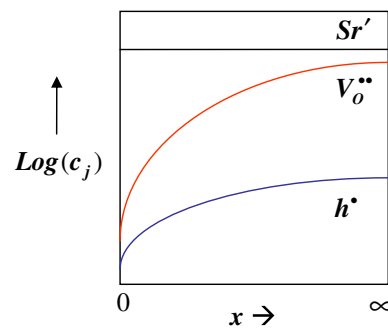

Fig. 3 Concentration profiles (qualitative) of the dopant (Sr'), oxygen vacancies ($V_O^{\bullet\bullet}$) and electron holes ($h^{\bullet}$) at grain boundaries in LSGO as expected from a space-charge model when $\phi(0) > 0$. Note that $t_{el,gb}$ is greater than $t_{el,\infty}$
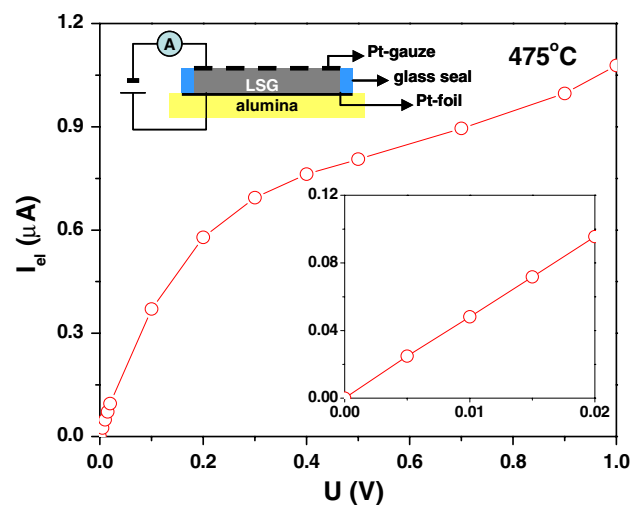

Fig. 4 The current (I)–voltage (U) characteristics measured from an ion-blocking dc-polarization cell. The *inset in the upper-left corner* shows a schematic diagram of the cell. The reversible electrode was exposed to air

separately. Prior to measuring the I–U characteristics, the ion-blocking cell was polarized at a constant applied voltage of 5 mV. During polarization, the initial current (~ 155 nA) rapidly dropped to reach an equilibrium value of 30 nA within 1000 s. This fact ensures that the ionic current is effectively blocked at the ion-blocking electrode. Figure 4 shows that the current linearly increases with increasing applied voltage up to ~ 25 mV and then starts to deviate from linear behavior to show the characteristic nonlinear I–U relation for a blocking cell as the voltage further increases. In light of the fact that the concentration of electrons in LSGO in the P_{O_2} range of concern is negligibly small compared to that of h$^{\cdot}$ (i.e., h$^{\cdot}$ is almost exclusively responsible for the electronic current in LSGO, if not entirely), one can estimate the partial electronic conductivity ($\sigma_{el} = 1/R_{el}(d/A)$, where d and A are the distance between the electrodes and the area of the electrode, and R denotes resistance) by directly measuring R_{el} in the ohmic region (<25 mV).

It is also necessary for one to selectively measure the local σ_{el} in the bulk and at the grain boundaries to eventually estimate both $t_{el,gb}$ and $t_{el,\infty}$. This is actually possible owing to the fact that the activation energy of R_{gb} (~ 0.7 eV) estimated from the Arrhenius plots (not shown here) was found to be significantly higher than that of R_{∞} (~ 1.4 eV) in LSGO [13, 14]. At relatively high temperatures (>750 °C), the resistance in LSGO is predominantly determined by R_{∞} (i.e., $R_{dc} = R_{\infty} + R_{gb} \approx R_{\infty}$ since $R_{\infty} \gg R_{gb}$), while R_{gb} is responsible for the resistance (i.e., $R_{dc} = R_{\infty} + R_{gb} \approx R_{gb}$ since $R_{\infty} \ll R_{gb}$) at lower temperatures (<500 °C) [14]. Note that the electrodes of the sample were modified in such a way that the resistance at the electrodes is negligibly small at all temperatures of concern [14] (also see "Experimental" for details). By measuring R_{el} in different temperature regions, one can thus measure $R_{el,\infty}$ and $R_{el,gb}$ selectively and thus $t_{el,\infty}$ and $t_{el,gb}$.

Figure 5 shows $t_{el,gb}$ and $t_{el,\infty}$ estimated at different temperatures. The $t_{el,gb}/t_{el,\infty}$ measured at lower/higher temperatures was extrapolated to higher/lower temperatures for direct comparison. As is clear from Fig. 5, $t_{el,gb}$ is greater than $t_{el,\infty}$ as expected from Fig. 2 at all temperatures of concern. Therefore, Fig. 5 verifies that the high grain-boundary resistance to oxygen-ionic transport observed in LSGO is due to the depletion of $V_O^{\cdot\cdot}$ to form space charge zones at the grain boundaries. Space-charge-controlled grain-boundary conduction in perovskites has been previously reported for dielectric oxides (e.g., acceptor-doped SrTiO$_3$), and intensively studied by Waser, Maier and their coworkers [18–23 and references cited therein]. At the grain boundaries in these materials, both $V_O^{\cdot\cdot}$ and h$^{\cdot}$ were found to be depleted, forming space-charge zones similar to those we observed in LSGO.
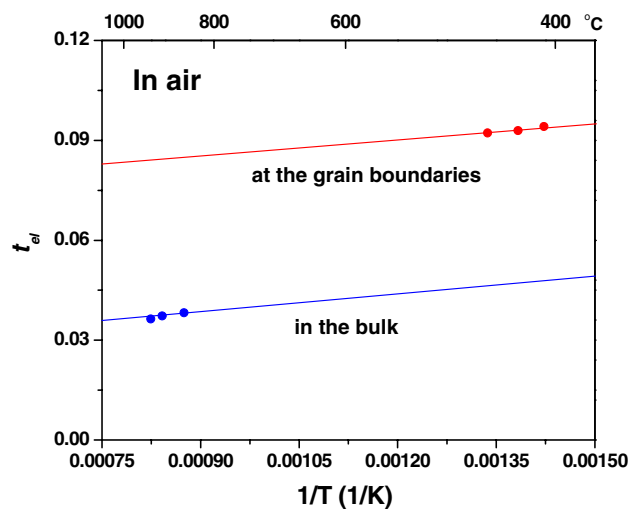
Fig. 5 The transference numbers for electron holes in the bulk (*blue symbols*) and at the grain boundaries (*red symbols*) measured at different temperatures. The *solid lines* indicate extrapolations of the measured data

A more quantitative and comprehensive analysis of the influence of space-charge effects on the oxygen-ionic transport in LSGO is given in [13]. Attention should also be paid to the origin of the grain-boundary resistance in highly doped LaGaO$_3$, materials that are more relevant to practical applications. In highly doped samples, the influence of space-charge effects on grain-boundary conduction may be less, since the width of the space-charge zone (related to the Debye length) decreases with increasing dopant concentration in the bulk. This issue is currently under investigation.

Experimental

One mol% Sr-doped LaGaO$_3$ (La$_{0.99}$Sr$_{0.01}$GaO$_{3-x}$: LSGO) was synthesized employing a Pechini-type method using La(NO$_3$)$_3 \cdot$ 6H$_2$O (99.9%, Sigma–Aldrich, St. Louis, MO, USA), Ga(NO$_3$)$_3 \cdot$ 8H$_2$O ($>$99.9%, Sigma–Aldrich) and Sr(NO$_3$)$_2$ (99.9%, Sigma–Aldrich) as reactants. The synthesized LSGO was pressed into pellets at 300 MPa by cold isostatic pressing. The as-pressed pellets were sintered at 1600 °C for 10 h in air. The relative density of the sintered pellets, estimated using an Archimedean method, was above 95%. The chemical composition as well as the concentrations of background impurities (including Ca and Si) in the pellets were determined using inductively coupled plasma emission spectroscopy (ICP). The structure and phase homogeneity of the LSGO pellets was characterized using an X-ray diffractometer (XRD) with Cu-K$_\alpha$ radiation (XDS 2000, Scintag, Santa Clara, CA, USA). No indication of secondary phase formation was observed.

The microstructure of the pellets was examined using a high-resolution transmission electron microscope (HR-TEM, JEM-2500SE, JEOL, Tokyo, Japan).

The electrical resistance of the pellet was measured as a function of temperature ($T = 250 \sim 600$ °C) under different oxygen partial pressures using both two-probe ac impedance spectroscopy and a dc-measurement technique. Prior to the measurements, Pt electrodes were fabricated by painting Pt paste (5349, Heraeus, Hanau, Germany) on both surfaces of the pellet, followed by annealing at 1000 °C/1 h in air. Impedance spectra were obtained in the frequency range from 50 mHz to 10 MHz using an impedance analyzer (Novocontrol, Novocontrol Technology, Hundsangen, Germany). The total dc currents were measured using a source-measure unit (236, Keithley, Cleveland, OH, USA) in the high-temperature (≥ 750 °C) and the low-temperature (≤ 500 °C) regions. To minimize the electrode resistance of the pellet, which may be present at low temperatures, the surfaces of the pellets were coated with a porous composite layer. The composite material was prepared by mechanically mixing LSG and LSM ($La_{0.8}Sr_{0.2}MnO_{3-\delta}$, FCM, USA) powders (1:1 wt%) with the organic solvent. The slurry was screen-printed on the surface of the pellet and then heated at 1000 °C for 2 h in air.

The partial electronic current in the sample was measured using a dc-polarization method. A dc source meter (230, Keithley) was used to apply constant voltage (U) from 0 V to 1.0 V, and an electrometer (617, Keithley) was used to measure the current (I).

References

1. Maier J (2000) Point-defect thermodynamics and size effects. Solid State Ionics 131:13
2. Goodenough JB (2003) Oxide-ion electrolytes. Ann Rev Mat Res 33:91
3. Minh NQ (1993) Ceramic fuel-cells. J Am Ceram Soc 76(3):563
4. Steele BCH (2000) Materials for IT-SOFC stacks 35 years R&D: the inevitability of gradualness? Solid State Ionics 134(1–2):3
5. Guo X, Maier J (2001) Grain boundary blocking effect in zirconia: a Schottky barrier analysis. J Electrochem Soc 148(3):E121
6. Lee JS, Anselmi-Tamburini U, Munir ZA, Kim S (2006) A direct evidence of electron accumulation in the grain boundary of yttria doped nanocrystalline zirconia ceramics. Electrochem Solid-State Lett L9(8):J34
7. Kim S, Maier J (2002) On the conductivity mechanism of nanocrystalline ceria. J Electrochem Soc 149:J73
8. Tschoepe A (2001) Grain size-dependent electrical conductivity of polycrystalline cerium oxide II: space charge model. Solid State Ionics 139:267
9. Guo X, Waser R (2006) Electrical properties of the grain boundaries of oxygen ion conductors: acceptor-doped zirconia and ceria. Prog Mater Sci 51:152
10. Maier J (1995) Ionic conduction in space charge regions. Prog Solid State Chem 23:171
11. Kim S, Fleig J, Maier J (2003) Space charge conduction: simple analytical solutions for ionic and mixed conductors and application to nanocrystalline ceria. Phys Chem Chem Phys 5:2268
12. Ishihara T, Matsuda H, Takita Y (1994) Doped $LaGaO_3$ perovskite-type oxide as a new oxide ionic conductor. J Am Chem Soc 116(9):3801
13. Park HJ, Kim S (2007) Space charge effects on the interfacial conduction in Sr-doped lanthanum gallates: a quantitative analysis. J Phys Chem C 111:14903
14. Park HJ, Kim S (2008) The enhanced electronic transference number at the grain boundaries in Sr-doped $LaGaO_3$. Solid State Ionics 179:1329
15. Slater PR, Irvine JTS, Ishihara T, Takita Y (1998) The structure of the oxide ion conductor La0.9Sr0.1Ga0.8Mg0.2O2.85 by powder neutron diffraction. Solid State Ionics 107:319
16. Hebb MH (1952) Electrical conductivity of silver sulfide. J Chem Phys 20:185
17. Wagner C (1955) Galvanische Zellen mit festen Elektrolyten mit gemischter Stromleitung. Z Elektrochem 60:4
18. Volmamm M, Waser R (1994) Grain-boundary defect chemistry of acceptor-doped titanates—space-charge layer width. J Am Ceram Soc 77:235
19. Waser R (1995) Electronic-properties of grain-boundaries in $SrTiO_3$ and $BaTiO_3$ ceramics. Solid State Ionics 75:89
20. Waser R, Hagenbeck R (2000) Grain boundaries in dielectric and mixed conducting ceramics. Acta Mater 48:797
21. Denk I, Claus J, Maier J (1997) Electrochemical investigations of $SrTiO_3$ boundaries. J Electrochem Soc 144:3526
22. Leonhardt M, Jamnik J, Maier J (1999) In situ monitoring and quantitative analysis of oxygen diffusion through Schottky-barriers in $SrTiO_3$ bicrystals. Electrochem Solid-State Lett 2:333
23. De Souza RA, Zehnpfenning J, Martin M, Maier J (2005) Determining oxygen isotope profiles in oxides with Time-of-Flight SIMS. Solid State Ionics 176:1465